



Emergence of negative viscosities and colored noise under current-driven Ehrenfest molecular dynamics

Riley J. Preston, Thomas D. Honeychurch, and Daniel S. Kosov 

College of Science and Engineering, James Cook University, Townsville, QLD 4811, Australia

 (Received 19 April 2022; revised 26 October 2022; accepted 31 October 2022; published 7 November 2022)

Molecules in molecular junctions are subject to current-induced forces that can break chemical bonds, induce reactions, destabilize molecular geometry, and halt the operation of the junction. Theories behind current-driven molecular dynamics simulations rely on a perturbative timescale separation within the system with subsequent use of nonequilibrium Green's functions (NEGF) to compute conservative, nonconservative, and stochastic forces exerted by electrons on nuclear degrees of freedom. We analyze the effectiveness of this approximation, paying particular attention to the phenomenon of negative viscosities. The perturbative approximation is directly compared to the nonequilibrium Ehrenfest approach. We introduce a time-stepping approach to calculate the forces present in the Ehrenfest method via exact integration of the equations of motion for the nonequilibrium Green's functions, which does not necessitate a timescale separation within the system and provides an exact description for the corresponding classical dynamics. We observe that negative viscosities are not artifacts of a perturbative treatment but also emerge in Ehrenfest dynamics. However, the effects of negative viscosity have the possibility of being overwhelmed by the predominantly positive dissipation due to the higher order forces unaccounted for by the perturbative approach. Additionally, we assess the validity of the white-noise approximation for the stochastic forces, finding that it is justifiable in the presence of a clear timescale separation and is more applicable when the current-carrying molecular orbital is moved outside of the voltage window. Finally, we demonstrate the method for molecular junction models consisting of one and two classical degrees of freedom.

DOI: [10.1103/PhysRevB.106.195406](https://doi.org/10.1103/PhysRevB.106.195406)

I. INTRODUCTION

The prototypical building block of nanoscale electronics technology is the molecular junction, in which a chosen molecule is bonded between two conducting leads. Current densities in nanoscale electronic devices far outweigh that of their macroscopic counterparts [1]. This results in joule heating [2–13] whereby energy from the tunneling electrons is transferred to the vibrational degrees of freedom of the molecule. This can result in a plethora of technologically unwanted but physically interesting effects such as large-scale conformational changes of the molecule which affect the conduction properties of the system [14,15], as well as total bond rupture and device breakdown [3,16–21]. Clearly it is desirable for us to be able to predict and even manipulate such behaviors to our advantage, emphasizing the need for reliable theoretical models which accurately describe the interplay between electronic and vibrational degrees of freedom.

The prevailing theory can be partitioned into two main archetypes; methods which opt to treat the entire system on a quantum footing, and quasiclassical methods which utilize a classical description of nuclei interacting with a quantum environment. Purely quantum models of the molecular dynamics are often limited to harmonic vibrations [22–26] or other generic vibrational potentials [27,28] which are unaffected by the electronic environment. Other quantum methods which are able to accurately account for the large-scale motion required

to study device breakdown are generally limited to highly simplistic systems with minimal relevance to experiment or are computationally infeasible to simulate [29–31]. It is instead convenient to adopt a quasiclassical approach in which the nuclei are assumed to behave according to classical equations of motion under the effects of the quantum tunneling electrons. This enables the description of arbitrary molecular potentials for systems along with being able to capture experimentally observed phenomena such as current-induced heating [32–37] along with bond rupture and electronically induced chemical reactions [38–41], at the cost of a fully quantum description.

A common accompanying assumption is the clear separation of timescales between the classically described nuclei and the electronic environment, which through the use of a perturbative approximation allows for a Langevin description of the classical particle [32–36,41–48]. In this regime, the particle dynamics are described by stochastic differential equations in which nuclei evolve under the influence of a frictional force which acts to subdue nuclear vibrations, and a stochastic force which delivers energy to the nuclei; the balance of these two forces yielding the effective temperature of the molecule. In addition, the influence of the electronic environment on the molecular potential is captured by an additional, typically nonconservative [49–51], renormalization term which can naturally describe switching phenomena and bond stability [32,35,41,44]. The Langevin approach has had great success in the description and simulation of large-scale

systems corresponding to real molecular electronic junction configurations, such as for graphene nanoribbons [52,53].

One such theoretically predicted phenomenon which leads to device breakdown is the notion of a negative dissipation; under a Langevin approach, this implies that the viscosity coefficient becomes negative [32,36,44,47,54–56]. In this regime, energy is applied to rather than dissipated from the classical coordinate until it reaches unsustainable temperatures for the device. Negative dissipations have also been predicted using purely quantum mechanical methods in which a population inversion in the quantized phonons leads to ever-increasing temperatures [46,57–62]. The physicality of such theoretical results have often been called into question, thought to arise as an artifact of assumptions applied in the theory rather than a demonstration of real behavior [63].

In this paper we extend the quasiclassical formalism by utilizing a numerically exact method to calculate the forces acting on our classical coordinates without resorting to the assumption of a timescale separation within the system. This is commonly known as the Ehrenfest approach to classical dynamics and it has garnered significant interest in the modeling of nuclear motion in nanoscale systems [38,49–51,55,56,64–68]. This approach treats the electron-nuclear interaction on a mean-field level; it therefore does not provide a full description of the inelastic scattering between electrons and nuclei and cannot fully capture the effects of joule heating within the system [65,66,69–71]. Efforts have been made to remedy these caveats via perturbative corrections to the electron-nuclear correlations with some success [70,71]. However, in this study we seek only to utilize Ehrenfest dynamics as a basis for comparison for predictions made by the perturbative Langevin approach. In doing so, we once again observe the emergence of negative dissipations and validate the results of the perturbative Langevin approximation, depending on the parameter range applied.

Our approach additionally allows for the exploration of the autocorrelations in the stochastic force. In general, the stochastic force is correlated at different times dependent on the electronic structure of the system considered; this corresponds to colored noise [45,72,73]. The correlations are additionally dependent on the nonadiabatic motion of the classical coordinate. However, it is often computationally infeasible to account for colored noise and it becomes necessary to employ a white-noise approximation. Under this approximation, the colored-noise diffusion is replaced by a Markovian, white-noise equivalent which attempts to produce the same dynamical behavior [32,33,39,41,42,44]. We apply our method to investigate the effects of a timescale separation on the diffusion coefficient along with assessing the validity of the white-noise approximation to the diffusion under a variety of regimes.

In Sec. II we introduce the theory which describes the classical dynamics. This involves the introduction of the Ehrenfest force along with its corresponding perturbative Langevin approximation, both expressed in terms of nonequilibrium Green's functions. We also discuss our iterative method for evaluating the Ehrenfest force through time. In Sec. III B we demonstrate the accuracy of the perturbative approximation for a simple system consisting of a single classical degree of freedom, while in Sec. III C we then apply Ehrenfest dynamics

to a system with two classical degrees of freedom. Finally, in Sec. III D we utilize our method to evaluate the diffusion coefficient and the suitability of the white-noise approximation for the stochastic force over a range of parameters. We use atomic units for all parameters and results presented.

II. THEORY

A. Hamiltonian

Our system is described by a generic tunneling Hamiltonian as per

$$H(t) = H_M(t) + H_L + H_R + H_{LM} + H_{MR} + H_{cl}(t). \quad (1)$$

The total system Hamiltonian is partitioned into the following components; the molecular Hamiltonian $H_M(t)$, the left and right leads Hamiltonians H_L and H_R , the leads-molecule coupling Hamiltonians H_{LM} and H_{MR} which describe the coupling between the electronic states on the central molecule and the left and right leads, respectively, and the classical Hamiltonian H_{cl} which describes the time-evolving molecular geometry.

The molecular Hamiltonian takes the form

$$H_M(t) = \sum_{ij} h_{ij}[\mathbf{x}(t)] d_i^\dagger d_j, \quad (2)$$

where the operators d_i^\dagger and d_j denote the creation and annihilation operators for the atomic electronic states whose energies are given by the diagonal Hamiltonian matrix elements $h_{ii}[\mathbf{x}(t)]$ while the hopping amplitudes are given by $h_{ij}[\mathbf{x}(t)]$. Note the explicit time dependence here, which arises as a result of the time evolution of the multidimensional classical coordinate \mathbf{x} . We will usually not show the time dependence of \mathbf{x} explicitly.

The lead Hamiltonian is taken in the standard form:

$$H_L + H_R = \sum_{k\alpha} \epsilon_{k\alpha} d_{k\alpha}^\dagger d_{k\alpha}, \quad (3)$$

where the creation and annihilation operators are given by $d_{k\alpha}^\dagger$ and $d_{k\alpha}$, and the subscript $k\alpha$ denotes the operator acting on state k in the α lead which has energy $\epsilon_{k\alpha}$.

The system-lead coupling Hamiltonians H_{LM} and H_{MR} are given by

$$H_{LM} + H_{MR} = \sum_{k\alpha i} (t_{k\alpha i} d_{k\alpha}^\dagger d_i + \text{H.c.}). \quad (4)$$

The matrix elements $t_{k\alpha i}$ (and their conjugates) describe the tunneling amplitudes between lead states $k\alpha$ and the molecular orbitals i . We take $t_{k\alpha i}$ to be independent of \mathbf{x} .

Finally, the classical Hamiltonian is given by

$$H_{cl}(t) = \sum_v \frac{p_v^2}{2m_v} + U(\mathbf{x}), \quad (5)$$

where the summation is taken over all classical degrees of freedom. The classical momentum for the ν degree of freedom is given by p_ν , while m_ν is the corresponding mass and $U(\mathbf{x})$ is the multidimensional potential.

B. Forces on the classical coordinate

The force operator for the force acting on the classical coordinates due to the quantum environment is given by

$$\mathbf{f}(t) = -\nabla H(t) \quad (6)$$

$$= -\nabla H_M(\mathbf{x}) - \nabla U(\mathbf{x}), \quad (7)$$

where $\nabla = [\partial_{v_1}, \partial_{v_2}, \dots]^T$ and ∂_{v_i} is the partial derivative with respect to the classical coordinate v_i . We have retained only the Hamiltonian components which depend on the classical coordinates. By taking the quantum average of the force operator, we introduce the so-called Ehrenfest force according to

$$\mathbf{F}^{\text{ehr}}(t) = -\langle \nabla H_M(\mathbf{x}) \rangle. \quad (8)$$

This is the main object of the present study. As discussed, the Ehrenfest force alone is ill-equipped to capture the entirety of the dynamics of the system. In order to completely describe the classical motion, an additional stochastic force term is required according to

$$f_\nu(t) = -\partial_\nu U + F_\nu^{\text{ehr}}(t) + \delta f_\nu(t), \quad (9)$$

where the subscript ν denotes the force acting on the ν classical degree of freedom. This equation can be obtained by taking the classical limit of the Feynman-Vernon influence functional for a system interacting with a quantum environment and applying a Hubbard-Stratonovich transformation, in which the dynamical evolution is split into a deterministic (Ehrenfest) component and a stochastic component [45,74]. For the purposes of our simulations, we disregard the stochastic component in (9) and instead focus solely on the Ehrenfest force along with the classical force arising from U since an accurate description of joule heating is not the aim of this study. We separately consider the influence of the stochastic force in Sec. III D. We choose to model the classical potential for any degree of freedom according to a harmonic potential as given by

$$U(\mathbf{x}) = \sum_\nu \frac{1}{2} k_\nu (v - v_0)^2, \quad (10)$$

where k_ν is the spring constant for the ν degree of freedom, and v_0 is a parameter which shifts the potential along the ν coordinate. The model is not restricted to this choice of potential; it is capable of dealing with arbitrary classical potentials. Our primary tool for evaluating the forces is the nonequilibrium Green's function. For our Hamiltonian, the Ehrenfest force can be represented in terms of the lesser component of exact nonequilibrium Green's functions as

$$F_\nu^{\text{ehr}}(t) = i\text{Tr}\{\partial_\nu h(t)G^<(t, t)\}, \quad (11)$$

where h contains the elements of the molecular Hamiltonian and the elements of $G^<$ are defined according to

$$G_{ij}^<(t, t') = i\langle d_j^\dagger(t')d_i(t) \rangle. \quad (12)$$

Each are square matrices with dimension corresponding to the number of molecular electronic energy levels.

C. Perturbative expansion of the Ehrenfest force

By enforcing a timescale separation between the classical degrees of freedom and the electronic environment, a perturbative expansion of the Ehrenfest force can be taken, from which we can derive the Langevin description of dynamics [32–34,36,41,42,44,47]. Here our small parameter is Ω/Γ , where Ω is the characteristic classical vibrational frequency and $1/\Gamma$ is associated with the electron tunneling time in molecular electronic junctions [1]. This amounts to assuming that the classical coordinate vibrates over much longer timescales than the time an electron spends in the central region. This interpretation is appropriate for the systems considered in our paper. Γ is generally a highly tunable experimental parameter while Ω depends on the vibrational mode considered. In order to identify the separate timescales, we introduce Wigner coordinates for the time. These are the central time (T) and relative time (τ) which are defined according to

$$T = \frac{t+t'}{2}, \quad \tau = t-t'. \quad (13)$$

We then define an auxiliary force $\mathcal{F}(t, t')$ which is equal to $F^{\text{ehr}}(t)$ when $t = t'$. Thus, we have

$$\mathcal{F}(t, t') = i\text{Tr}\{\partial_\nu h(t)G^<(t, t')\}. \quad (14)$$

Application of the Wigner transform along with its inverse results in

$$\mathcal{F}(t, t') = i\text{Tr}\left\{\int \frac{d\omega}{2\pi} e^{-i\omega\tau} \partial_\nu h(T)\tilde{G}^<(T, \omega)\right\}, \quad (15)$$

where G denotes a Green's function in the time domain, and \tilde{G} denotes the Wigner space defined as

$$\tilde{G}(T, \omega) = \int d(t-t') e^{i\omega(t-t')} G(t, t'). \quad (16)$$

We adopt the convention that if the integral limits are not shown explicitly, they range from $-\infty$ to ∞ . We will often subdue the (T, ω) indices for brevity. We now propose the ansatz

$$\tilde{G}^< = \tilde{G}_{(0)}^< + \tilde{G}_{(1)}^< + \tilde{G}_{(2)}^< + \dots, \quad (17)$$

in which $\tilde{G}_{(n)}^<$ is of n th order in our small parameter. Here $\tilde{G}_{(0)}^<$ is adiabatic and corresponds to the Born-Oppenheimer approximation, while the higher order terms go beyond this and account for the nonzero motion of the classical coordinates. Applying this ansatz and letting $t = t'$ finally yields

$$F_\nu^{\text{ehr}}(t) = i\text{Tr}\left\{\int \frac{d\omega}{2\pi} \partial_\nu h(t)(\tilde{G}_{(0)}^<(t, \omega) + \tilde{G}_{(1)}^<(t, \omega) + \dots)\right\} \quad (18)$$

$$= \underbrace{F_{\nu,(0)} + F_{\nu,(1)}}_{\text{retained in Langevin approach}} + F_{\nu,(2)} + \dots \quad (19)$$

Retaining only the zeroth (adiabatic) and first order contributions to the Ehrenfest force yields the deterministic forces present in the Langevin description, where the adiabatic force is purely position dependent while the first order force is the correction which accounts for nonzero velocities. The viscosity coefficient matrix $\hat{\xi}$ is obtained via

$$\mathbf{F}_{(1)} = -\hat{\xi}\mathbf{v}, \quad (20)$$

where $\hat{\xi}$ is an $n \times n$ matrix; n corresponding to the number of classical degrees of freedom in the system.

D. Solving for the adiabatic and first order Green's functions

The adiabatic and first order Green's functions in the frequency domain can be solved for via the Keldysh-Kadanoff-Baym equations, expressed in the Wigner space as [32,41,44]

$$\left(\omega + \frac{i}{2}\partial_T - e^{\frac{1}{2i}\partial_\omega^G \partial_T^h} h(T)\right) \tilde{G}^{R/A} = I + e^{\frac{1}{2i}(\partial_T^2 \partial_\omega^G - \partial_\omega^2 \partial_T^G)} \tilde{\Sigma}^{R/A} \tilde{G}^{R/A} \quad (21)$$

and

$$\begin{aligned} & \left(\omega + \frac{i}{2}\partial_T - e^{\frac{1}{2i}\partial_\omega^G \partial_T^h} h(T)\right) \tilde{G}^{</>} \\ & = e^{\frac{1}{2i}(\partial_T^2 \partial_\omega^G - \partial_\omega^2 \partial_T^G)} (\tilde{\Sigma}^R \tilde{G}^{</>} + \tilde{\Sigma}^{</>} \tilde{G}^A), \end{aligned} \quad (22)$$

where we have shown the retarded/advanced and the lesser/greater collectively. Here we adopt the convenient notation for derivatives ∂_T^G , which denotes a partial derivative acting on the G term with respect to T and so on. Again, each quantity here is a square matrix with dimensions corresponding to the number of electronic levels in the central region. Since T is associated with the motion of the classical coordinate, terms containing $(\partial_T)^n$ will be of n th in our small parameter. Thus, we apply our ansatz in (17), along with applying an expansion of the exponentials in orders of ∂_T . Truncating after the zeroth order and solving for $\tilde{G}_{(0)}$ yields the standard adiabatic Green's functions as follows:

$$\tilde{G}_{(0)}^{R/A} = (\omega \hat{I} - h - \tilde{\Sigma}^{R/A})^{-1}, \quad (23)$$

$$\tilde{G}_{(0)}^{</>} = \tilde{G}_{(0)}^R \tilde{\Sigma}^{</>} \tilde{G}_{(0)}^A. \quad (24)$$

An equivalent approach for the first order yields [32,41,44]

$$\tilde{G}_{(1)}^{R/A} = \frac{1}{2i} \tilde{G}_{(0)}^{R/A} [\tilde{G}_{(0)}^{R/A}, \partial_T h] \tilde{G}_{(0)}^{R/A}, \quad (25)$$

$$\begin{aligned} \tilde{G}_{(1)}^{</>} & = \tilde{G}_{(0)}^R \tilde{\Sigma}^{</>} \tilde{G}_{(1)}^A + \tilde{G}_{(1)}^R \tilde{\Sigma}^{</>} \tilde{G}_{(0)}^A \\ & + \frac{1}{2i} \tilde{G}_{(0)}^R (\partial_T h \tilde{G}_{(0)}^R \partial_\omega \tilde{\Sigma}^{</>} + \tilde{G}_{(0)}^{</>} \partial_T h + \text{H.c.}) \tilde{G}_{(0)}^A. \end{aligned} \quad (26)$$

The self-energy components in the frequency domain are given by

$$\tilde{\Sigma}_\alpha^R = -\frac{i}{2}\Gamma_\alpha, \quad \tilde{\Sigma}_\alpha^A = \frac{i}{2}\Gamma_\alpha, \quad (27)$$

$$\tilde{\Sigma}_\alpha^{<} = i f_\alpha(\omega) \Gamma_\alpha, \quad \tilde{\Sigma}_\alpha^{>} = -i[1 - f_\alpha(\omega)] \Gamma_\alpha. \quad (28)$$

Here $f_\alpha(\omega)$ is the Fermi-Dirac distribution which describes the α lead. In solving for the above, we have applied the wide-band approximation to the leads such that $\Gamma_\alpha(\omega) = \Gamma_\alpha$. The explicit expression for an element of Γ_α is

$$\Gamma_{c,c',\alpha} = 2\pi \rho_\alpha t_{c,\alpha}^* t_{c',\alpha}, \quad (29)$$

where ρ_α is the now constant density of states for the α lead, and $t_{c,\alpha}$ is the coupling strength between any state in the α lead and the central region electronic state c . We take Γ_α as a parameter for our model. In Eqs. (27) to (29) the full quantity can be obtained by taking a sum over the leads α . For example,

$$\Gamma_{c,c'} = \sum_\alpha \Gamma_{c,c',\alpha}. \quad (30)$$

E. Time-stepping approach to the evolution of the Green's function

Clearly, if we are able to calculate $G^{<}(t, t')$ at each time, then (11) allows us to readily calculate the Ehrenfest force without a need to resort to a perturbative approach involving timescale separation. Our method is based off of the seminal work of Jauho *et al.* in Ref. [75], from which we borrow the main defined quantities. A similar time-stepping solution to Ehrenfest dynamics was presented in Ref. [68]. However, our application of the approach as detailed in this section is more sophisticated and allows for better convergence and stability. In approaching these calculations, we borrow the main defined quantities from Ref. [75]. The lesser and greater Green's function in the time domain are given by the Keldysh equation,

$$G^{</>}(t, t') = \int dt_1 \int dt_2 G^R(t, t_1) \Sigma^{</>}(t_1, t_2) G^A(t_2, t'). \quad (31)$$

For the sake of clarity, in this section we will use (\dots) to denote a functional dependence, whereas $[\dots]$ will denote a term in the equation. Now we will take (31) and express the $\Sigma^{</>}$ term according to the inverse Wigner transform of (28). In the lesser case we find

$$G^{<}(t, t') = i \sum_\alpha \int dt_1 \int dt_2 G^R(t, t_1) \int \frac{d\omega}{2\pi} e^{-i\omega[t_1 - t_2]} f_\alpha(\omega) \Gamma_\alpha G^A(t_2, t') \quad (32)$$

$$= i \sum_\alpha \int dt_1 \int dt_2 G^R(t, t_1) \int \frac{d\omega}{2\pi} e^{-i\omega[t_1 - t_2]} f_\alpha(\omega) \Gamma_\alpha G^A(t_2, t) e^{i\omega[t - t_1]} e^{i\omega[t' - t_1]} \quad (33)$$

$$= i \sum_\alpha \int \frac{d\omega}{2\pi} f_\alpha(\omega) e^{i\omega[t' - t_1]} \int dt_1 e^{i\omega[t - t_1]} G^R(t, t_1) \Gamma_\alpha \int dt_2 e^{-i\omega[t' - t_2]} G^A(t_2, t') \quad (34)$$

$$= i \sum_\alpha \int \frac{d\omega}{2\pi} e^{-i\omega\tau} f_\alpha(\omega) A(\omega, t) \Gamma_\alpha A^\dagger(\omega, t'). \quad (35)$$

An equivalent derivation can be applied in the greater case to find

$$G^>(t, t') = -i \sum_{\alpha} \int \frac{d\omega}{2\pi} e^{-i\omega\tau} [1 - f_{\alpha}(\omega)] A(\omega, t) \Gamma_{\alpha} A^{\dagger}(\omega, t'). \quad (36)$$

Here we have defined the quantity

$$A(\omega, t) = \int dt_1 e^{i\omega[t-t_1]} G^R(t, t_1). \quad (37)$$

The evolution of G^R is found via the Kadanoff-Baym equation in the time domain:

$$\left(i \frac{\partial}{\partial t} - h(t) \right) G^R(t, t') = \delta(t - t') + \int dt_1 \Sigma^R(t, t_1) G^R(t_1, t'). \quad (38)$$

By utilizing the fact that

$$\Sigma^R(t, t') = -\frac{i}{2} \Gamma \delta(t - t'), \quad (39)$$

we can solve the general solution of (38) as

$$G^R(t, t') = -i \Theta(t - t') \hat{T} \exp \left\{ -i \int_{t'}^t dt_1 h(t_1) - \frac{1}{2} \Gamma [t - t'] \right\}. \quad (40)$$

Here \hat{T} is the time-ordering operator and Θ is the Heaviside step function. By substituting (40) into (37) we arrive at

$$A(\omega, t) = -i \int_{-\infty}^t dt_1 \hat{T} \exp \left\{ i\omega[t - t_1] - i \int_{t_1}^t dt_2 h(t_2) - \frac{1}{2} \Gamma [t - t_1] \right\}. \quad (41)$$

This is the quantity which we will iteratively evolve forwards in time, from which we can then extract $G^<$ via (35). We begin by applying a step Δt forwards in time to (41),

$$A(\omega, t + \Delta t) = -i \int_{-\infty}^{t+\Delta t} dt_1 \hat{T} \exp \left\{ i\omega[t + \Delta t - t_1] - i \int_{t_1}^{t+\Delta t} dt_2 h(t_2) - \frac{1}{2} \Gamma [t + \Delta t - t_1] \right\} \quad (42)$$

$$= -i \int_{-\infty}^t dt_1 \hat{T} \exp \left\{ i\omega[t + \Delta t - t_1] - i \int_{t_1}^{t+\Delta t} dt_2 h(t_2) - \frac{1}{2} \Gamma [t + \Delta t - t_1] \right\} - i \int_t^{t+\Delta t} dt_1 \hat{T} \exp \left\{ i\omega[t + \Delta t - t_1] - i \int_{t_1}^{t+\Delta t} dt_2 h(t_2) - \frac{1}{2} \Gamma [t + \Delta t - t_1] \right\} \quad (43)$$

$$= A^A(\omega, t + \Delta t) + A^B(\omega, t + \Delta t). \quad (44)$$

Here we have split A into A^A which reflects how the history before t informs the system at $t + \Delta t$, and A^B which contains the effects of the system from t to $t + \Delta t$. A^A can be further simplified by partitioning the inner integral as follows:

$$A^A(\omega, t + \Delta t) = -i \int_{-\infty}^t dt_1 \hat{T} \exp \left\{ i\omega\Delta t - i \int_t^{t+\Delta t} dt_2 h(t_2) - \frac{1}{2} \Gamma \Delta t \right\} \times \hat{T} \exp \left\{ i\omega[t - t_1] - i \int_{t_1}^t dt_3 h(t_3) - \frac{1}{2} \Gamma [t - t_1] \right\} \quad (45)$$

$$= \hat{T} \exp \left\{ i\omega\Delta t - i \int_t^{t+\Delta t} dt_2 h(t_2) - \frac{1}{2} \Gamma \Delta t \right\} A(\omega, t). \quad (46)$$

We will make the assumption that for a sufficiently small Δt , $h(t)$ can be approximated as being piecewise constant. Thus, at some time-step t_n we assume that for $t_n < t < t_{n+1}$ we have $h(t) = h(t_n)$. This entails that our time-step size should be sufficiently small in the computational implementation when calculating classical trajectories. This enables us to directly calculate the integrals over $h(t)$ appearing in (46) and (43) along with removing the time-ordering operators. We thus reexpress $A^A(\omega, t + \Delta t)$ and $A^B(\omega, t + \Delta t)$ according to

$$A^A(\omega, t + \Delta t) = \exp \left\{ i\Delta t \left(\omega - h(t) + \frac{i}{2} \Gamma \right) \right\} A(\omega, t) \quad (47)$$

and

$$A^B(\omega, t + \Delta t) = -i \int_0^{\Delta t} dt_2 \exp \left(\omega - h(t) + \frac{i}{2} \Gamma \right) \quad (48)$$

$$= -i(e^{\Lambda\Delta t} - I)\Lambda^{-1}, \quad (49)$$

where I is the identity matrix, and for cleanliness we have used $\Lambda = i[\omega - h(t) + \frac{i}{2}\Gamma]$. Here we have used the matrix exponential identity:

$$\int_0^T dt e^{Xt} = (e^{XT} - I)X^{-1}. \quad (50)$$

Now we have everything we need to be able to perform an Ehrenfest simulation of the classical dynamics. The algorithm functions as follows. First, we assume an adiabatic initial condition, such that (37) can be calculated through the use of (23). The initial force can then be computed according to (35) and (11) given the chosen initial conditions for the classical coordinate. The calculated Ehrenfest force feeds into an external algorithm which updates the nuclear dynamics to the next time step, at which point we use (47) and (49) to nonadiabatically compute A at the next time step. From here

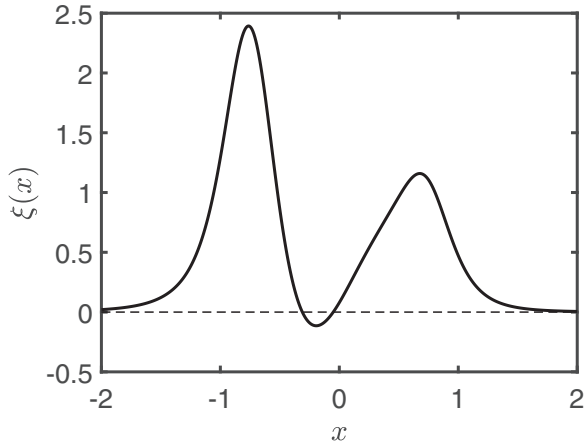


FIG. 1. The viscosity coefficient as a function of the classical coordinate. Atomic units are used for quantities here and in all further plots in the paper.

the process repeats, yielding a wholly nonadiabatic, classical trajectory in time.

III. RESULTS

A. Purely positive viscosity in the single-level case

In the case where there is only a single electronic level in the central region and only the molecular Hamiltonian contains classical dependence, the diagonal components of the viscosity matrix ξ can be given by

$$\xi_{vv} = \frac{\Gamma(\partial_v h)^2}{4\pi} \int d\omega \frac{\frac{f_L}{T_L}(1-f_L)\Gamma_L + \frac{f_R}{T_R}(1-f_R)\Gamma_R}{[(\omega-h)^2 + \Gamma^2/4]^2}, \quad (51)$$

where T_L and T_R are the temperatures for the left and right lead, respectively. In our model we set $T_L = T_R = 0.001$. A rigorous derivation of (51) has been relegated to Appendix A. Thus, we observe that the diagonal viscosity elements are purely positive as each term in (51) is positive. From a Langevin standpoint, theory is known to produce negative viscosities in nonequilibrium in the case of multiple electronic levels [44,47,54], as well as resulting from non-Condon effects in which the geometry at the leads interface becomes relevant [32]. Due to the cumbersome nature of the equations in the latter case, we focus only on the former in this paper.

B. Single classical degree of freedom

Here we present results for a two-level system with a single classical degree of freedom. The matrix elements of the molecular Hamiltonian take the form

$$H_M = \begin{pmatrix} -\lambda x & \eta \\ \eta & \lambda x \end{pmatrix}, \quad (52)$$

where the classical coordinate x has the effect of linearly shifting the two atomic orbitals and η dictates the overlap. We choose the left lead to be coupled to the first state and the right lead to be coupled to the second state which gives our Γ

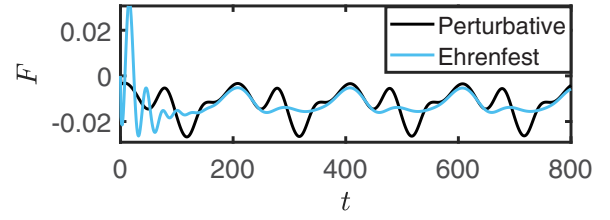


FIG. 2. Trajectory in time of $F^{\text{ehr}}(t)$ (Ehrenfest) and $F_{(0)}(t) + F_{(1)}(t)$ (perturbative). $\Omega/\Gamma \approx 0.32$.

matrices the following form:

$$\Gamma_L = \begin{pmatrix} \gamma & 0 \\ 0 & 0 \end{pmatrix}, \quad \Gamma_R = \begin{pmatrix} 0 & 0 \\ 0 & \gamma \end{pmatrix}. \quad (53)$$

In this section the common parameters are $\lambda = \eta = 0.1$, $\gamma = 0.05$, $k = 1$, $x_0 = -0.22$, and $\mu_L = -\mu_R = 0.12$, where μ_α is the chemical potential of the α lead. In contrast to the single-level case, this model allows us to observe negative viscosities. An example of this is shown in Fig. 1 where the coordinate dependent viscosity coefficient (now a scalar function in the case of a single classical degree of freedom) becomes negative in a small region around $x \approx -0.2$.

By utilizing our time-stepping algorithm to evolve $G^<$ in time as presented in Sec. II E we can calculate the Ehrenfest force as a function of time, from which we can then computationally simulate the dynamics of the classical coordinate. In Fig. 2 we calculate a classical Ehrenfest trajectory and record F^{ehr} at each time step. We also record the corresponding forces which the classical coordinate would experience under the perturbative truncation of F^{ehr} after the first order. We note that the methods clearly differ in the transient

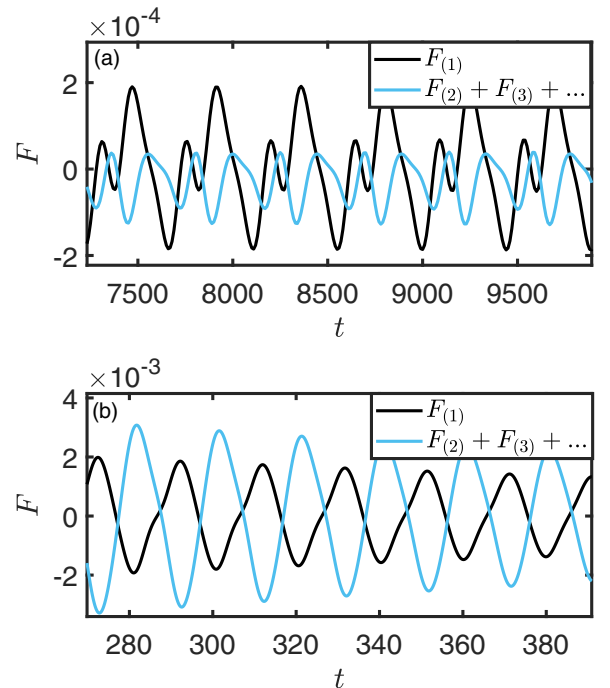


FIG. 3. Comparison of the first order force against the sum of all higher order forces. (a) $\Omega/\Gamma \approx 0.14$, (b) $\Omega/\Gamma \approx 3.2$.

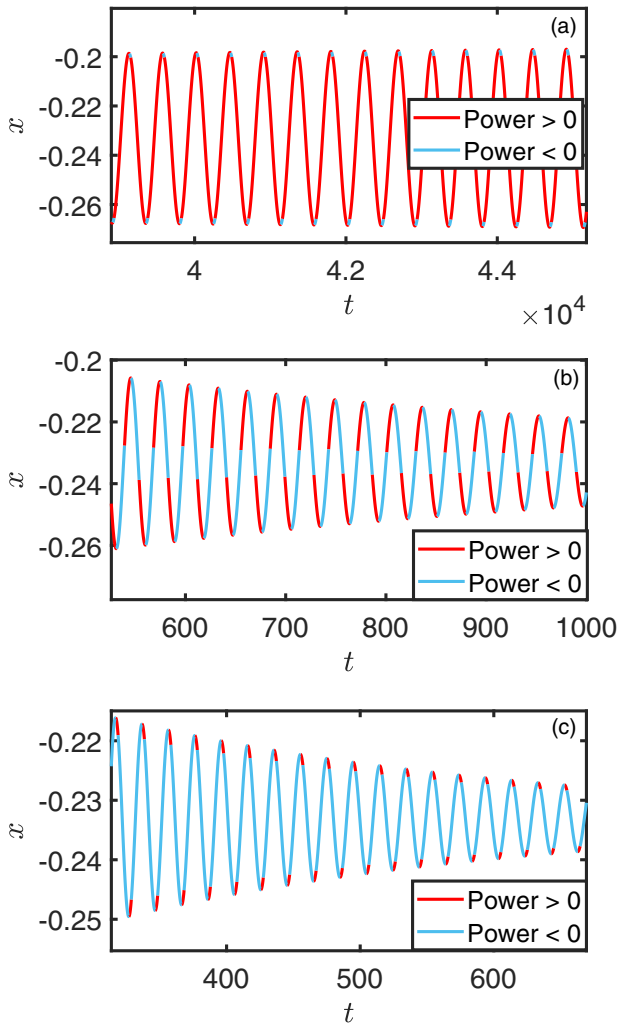


FIG. 4. Samples of Ehrenfest trajectories of the classical coordinate against time for (a) $\Omega/\Gamma \approx 0.14$, (b) $\Omega/\Gamma \approx 2.2$, and (c) $\Omega/\Gamma \approx 3.2$. Color shows the instantaneous power of the classical coordinate.

regime depending on the chosen initial conditions, before each settles into periodicity as the coordinate oscillates in time. The cause of the differences between the calculated Ehrenfest and perturbative forces are made clearer in Fig. 3, where a direct comparison has been made of the magnitude of the first order force relative to the sum of all higher order forces ($F_{(2)} + F_{(3)} + \dots$) for different values of Ω/Γ . This is achieved by varying the effective mass of the classical coordinate while keeping all other parameters constant. We can then estimate Ω by assuming that the oscillations are approximately harmonic. We observe that when Ω/Γ is small in Fig. 3(a), the higher order forces have only a small relative contribution. In Fig. 3(b) however, Ω/Γ is no longer small and thus our perturbative assumption is no longer satisfied, meaning the higher order forces have become increasingly relevant.

Calculation of the time-dependent forces allows us to then simulate the phase-space trajectory of the classical coordinate as a function of time. Figure 4 shows time-dependent trajectories of the classical coordinate x for three different values of

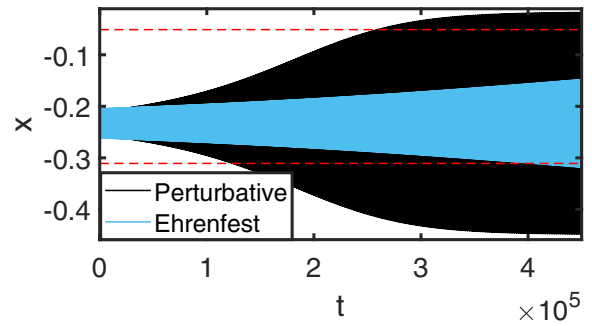


FIG. 5. Comparison of long trajectories of the classical coordinate in time using the Ehrenfest approach and the truncated perturbative approach. The viscosity coefficient is negative between the red dashed lines and positive outside. $\Omega/\Gamma \approx 0.14$.

the small parameter Ω/Γ . We also calculate the instantaneous power of the classical coordinate at each time step according to $(F^{\text{ehr}} - F_{(0)})_m^L$, which includes only the effects of the excitational and dissipative forces. The classical coordinate is intentionally confined to the region of negative viscosity shown in Fig. 1 via our choice of $U(x)$ such that under the perturbative assumption, the instantaneous power will be positive at all time steps. We observe that when $\Omega/\Gamma \ll 1$ as in Fig. 4(a); rendering the perturbative approximation as valid, the instantaneous power is overwhelmingly positive in agreement with the perturbative approximation. This entails that the oscillations will increase until reaching regions of positive viscosity, whereby they will form a limit cycle. This is further illustrated in Fig. 5 via long trajectories for the same parameters, where the amplitude of oscillations increases in both the Ehrenfest and perturbative approaches. This result demonstrates that even in the absence of timescale separation, negative viscosities emerge and dictate the behavior of the system. However, we observe the resultant trajectories from the two methods diverge from each other over longer timescales, demonstrating the importance of the higher order forces even for these parameters where we expect they can be reasonably neglected. We note that Ehrenfest dynamics has been used to observe the effects of negative viscosities in different regimes in the literature [55,56,62,68]. In Figs. 4(b) and 4(c), where $\Omega/\Gamma > 1$ and our perturbative assumption is no longer adequate, we observe that instantaneous power is more often negative, wherein the electronic environment is taking energy away from the classical coordinate. This means that the higher order terms (second order and above) in our perturbative expansion for F^{ehr} have become more relevant and the dissipative nature of these forces are overwhelming the negative viscosity produced by $F_{(1)}$. These results are summarized in Fig. 6 in which the aver-

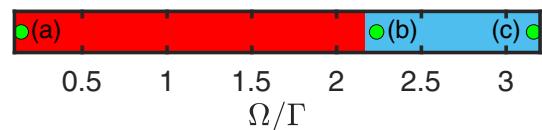


FIG. 6. Regimes of negative (blue) or positive (red) average power input to the classical coordinate over a period of oscillation. The green points refer to the corresponding plots in Fig. 4.

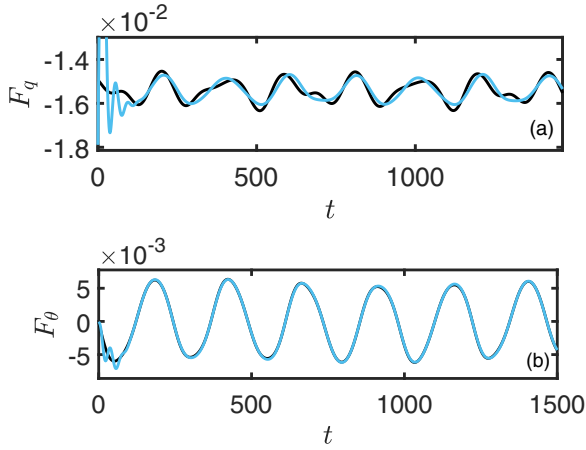


FIG. 7. The force trajectories in time for the Ehrenfest force (blue) and perturbative force (black) acting on (a) q and (b) θ . $\Omega_q/\Gamma \approx 0.32$, $\Omega_\theta/\Gamma \approx 0.22$.

age power input to the classical coordinate over a period of oscillation is calculated and classified as negative (blue) or positive (red). We observe that the average power input to the classical coordinate is positive far beyond when the perturbative assumption is valid. We anticipate that this cutoff between positive and negative average power input is highly dependent on the model and parameters at hand. However, this demonstrates that while negative viscosities will still emerge under a numerically exact approach, it can be dominated by dissipative higher order forces for large values of Ω/Γ . These results suggest that the inclusion of the higher order forces which emerge through Ehrenfest dynamics acts to further subdue classical vibrations within the system.

C. Two classical degrees of freedom

The algorithm for calculating F^{chr} can be readily extended to account for many classical degrees of freedom. In this section we consider another two-level model consisting now of two classical degrees of freedom; a stretching component and an angular component. As a result, in contrast to the case of a single vibrational degree of freedom, $F_{(0)}$ now becomes typically nonconservative. The stretching coordinate q modulates the hopping amplitude between electronic sites in the central region, while the angular coordinate θ accounts for the shift in electric levels due to the electric field produced by the applied voltage bias. Thus, the molecular Hamiltonian now takes the form

$$H_M = \begin{pmatrix} h_L(\theta) & \eta(q) \\ \eta(q) & h_R(\theta) \end{pmatrix}. \quad (54)$$

The hopping amplitude is given by

$$\eta(q) = \eta e^{-q}(1 + q + q^2/3). \quad (55)$$

This is a generic $1s$ -orbital overlap scaled by some constant η [76]. Meanwhile, the atomic levels are given by

$$h_{L/R}(\theta) = \pm E q_0 \cos(\theta), \quad (56)$$

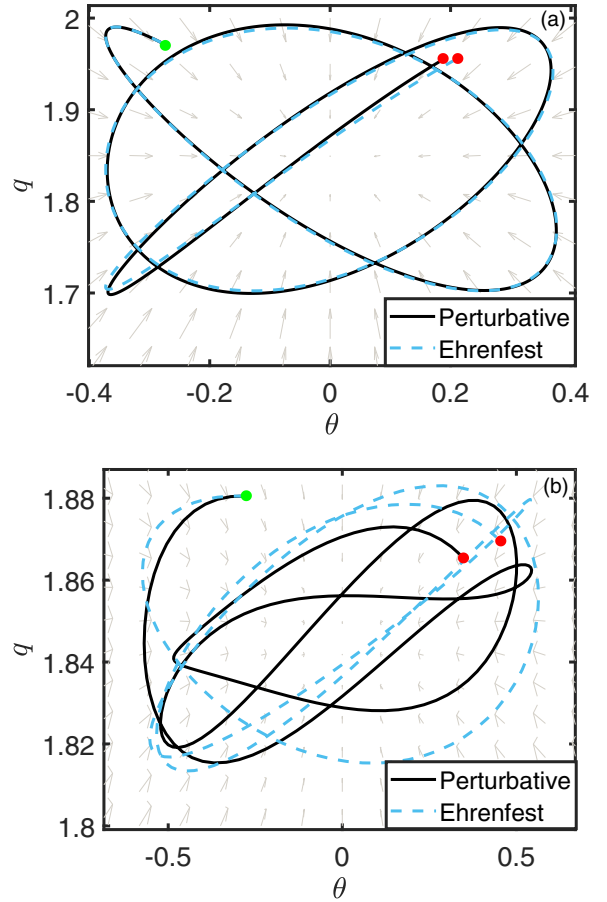


FIG. 8. Short classical trajectories in the coordinate space comparing the Ehrenfest method and perturbative method. Green (red) points denote the start (end) of the trajectory. The vector field shows $F^{\text{cl}} + F_{(0)}$. (a) $\Omega_q/\Gamma \approx 0.32$, $\Omega_\theta/\Gamma \approx 0.22$, and a trajectory length of 600, and (b) $\Omega_q/\Gamma = 1$, $\Omega_\theta/\Gamma \approx 0.7$, and a trajectory length of 200.

where q_0 is the constant bond-length parameter which appears in our classical potential for q , while E is the linear approximation to the electric field across the junction as determined by

$$E = \frac{\mu_L - \mu_R}{L}, \quad (57)$$

and L is the junction length. For all results in this section, we set $\eta = 0.1$, $q_0 = 2$, $\theta_0 = 0$, $L = 4$, $k_q = 0.1$, $k_\theta = 0.05$, and $\mu_L = -\mu_R = 0.1$. All other components of the full Hamiltonian take the same form as in Sec. III B.

In Fig. 7 we calculate an Ehrenfest trajectory and record the Ehrenfest and perturbative forces on each degree of freedom separately. Given that we have more than one classical degree of freedom, this also includes the so-called nonequilibrium antisymmetric forces in which the motion of θ induces a force on q and vice versa; the net antisymmetric force being perpendicular to the motion of the classical coordinate. Figure 8 performs a direct comparison between the time-dependent trajectories calculated via the Ehrenfest force and the perturbative approximation. To do so, we first calculate a classical Ehrenfest trajectory of our two coordinates. From

this trajectory at some point in time after the unusual transient behavior in F^{ehf} has subsided, we extract the initial conditions for a comparative trajectory where the forces are calculated according to the perturbative approximation. In Fig. 8(a) the trajectories are compared for large effective masses for each coordinate such that the perturbative assumption should be satisfied. We observe only small differences between the trajectories resulting from the different methods in this case. Contrarily, Fig. 8(b) demonstrates for small effective masses that the trajectories deviate away from each other almost instantly and undergo largely different oscillatory behavior. This is because the perturbative assumption is no longer valid since Ω/Γ is not sufficiently small.

D. Evaluating the diffusion coefficient

The stochastic force term which we have thus far avoided in (9) is a stochastic Gaussian process entirely defined by the following [45]:

$$\langle \delta f(t) \rangle = 0, \quad \langle \delta f(t) \delta f(t') \rangle = D(t, t'), \quad (58)$$

where we will refer to $D(t, t')$ as the exact diffusion coefficient. We will consider a system consisting of a single electronic level coupled to a single classical degree of freedom. Our molecular Hamiltonian is given by

$$H_M = h_0 + \lambda x, \quad (59)$$

where x represents any generic classical degree of freedom. We will let $h_0 = 0$ and our Γ_α become scalar inputs in the single level case. The exact diffusion coefficient in (58) for our model can then be expressed in terms of nonequilibrium Green's functions according to

$$D(t, t') = \lambda^2 G^>(t, t') G^<(t', t). \quad (60)$$

A derivation of this result is presented in Appendix B. Our $D(t, t')$ here is not exclusively real. Since our stochastic force is classical, we symmetrize (60) by taking the real component such that our expression for $D(t, t')$ is now in correspondence with Ref. [45] as per

$$D(t, t') = \text{Re}\{\lambda^2 G^>(t, t') G^<(t', t)\}. \quad (61)$$

$D(t, t')$ accounts for the effects of the random fluctuations about the mean field of the electronic environment on the classical degrees of freedom along with accounting for the feedback of the classical coordinate on the electronic environment due to its motion. However, generally a timescale separation within the system is utilized in order to produce a perturbative solution to $D(t, t')$ in which the nonadiabatic feedback due to the motion of the classical coordinate is not included; in other words, the classical coordinate evolves adiabatically. We can solve for the adiabatic form of $D(t, t')$ by considering the Wigner transform of (60) and retaining only the adiabatic terms. With some work, which has been relegated to Appendix C, the Wigner transform of (60) can be expressed as

$$\tilde{D}(\omega, T) = \lambda^2 \int \frac{d\omega'}{2\pi} \tilde{G}^>(\omega + \omega', T) \tilde{G}^<(\omega', T). \quad (62)$$

We note that (62) is a result of the phonon self-energy derived in Ref. [47]. Now, the adiabatic diffusion is found by taking

$\tilde{G}^{(\prime)}$ to be our adiabatic Green's functions as in (24). The subsequent application of the inverse Wigner transform then yields the adiabatic diffusion in the time domain as

$$D_{(0)}(\tau, T) = \lambda^2 \int \frac{d\omega}{2\pi} e^{-i\omega\tau} \int \frac{d\omega'}{2\pi} \tilde{G}_{(0)}^>(\omega + \omega', T) \tilde{G}_{(0)}^<(\omega', T). \quad (63)$$

The adiabatic diffusion will serve as a base of comparison with the exact diffusion in order to analyze the effects of a timescale separation within the system. We additionally analyze the validity of the white-noise approximation for different parameters. The white-noise approximation is a method of coarse graining the diffusion coefficient which allows for a simpler mathematical and computational treatment. This is done by assuming that the colored-noise exact diffusion coefficient can instead be replaced by a white-noise equivalent according to

$$D(t, t') \equiv D^w(T) \delta(t - t'), \quad (64)$$

where we have introduced the white-noise diffusion coefficient D^w . Thus, the aim is to accurately reproduce the effects of the stochastic force under the assumption that it is entirely uncorrelated in time. In order to replicate the correct dynamics using this approximation, it can be shown that D^w must then take the form

$$D^w(t_f) = \int_{-t_f}^{t_f} d\tau D(t_f, \tau), \quad (65)$$

where to avoid ambiguity, t_f denotes a specific point along the trajectory. This is demonstrated in Appendix D. Equation (65) is just the Wigner transform of $D(t, t')$ where $\omega = 0$ such that D^w is independent of ω ; hence the name ‘‘white-noise’’ diffusion. Thus, the white-noise diffusion coefficient contains information about the correlations in the stochastic force but applies that information in a Markovian manner. A timescale separation can be applied to the white-noise diffusion in a similar way as previously, whereby the adiabatic white-noise diffusion is given by

$$D_{(0)}^w(t_f) = \int_{-t_f}^{t_f} d\tau D_{(0)}(t_f, \tau). \quad (66)$$

The adiabatic white-noise diffusion is the most commonly used approximation to the diffusion coefficient [32,41,44] and we note in passing that it satisfies a fluctuation-dissipation relation with (51) when $\partial_\nu h = \lambda$. The white-noise approximation is valid when correlations in the exact diffusion coefficient decay over timescales in which the effects of other forces present in the system (in our case, the Ehrenfest and the classical forces) are negligible. In order to quantify its validity, we introduce the correlation time defined according to

$$t_{\text{corr}}(t_f) = \frac{\int_{-t_f}^{t_f} d\tau D(t_f, \tau)}{D(t_f, \tau = 0)}. \quad (67)$$

This is a measure of the persistence of correlations in the stochastic force, independent of their strength. The numerator of (67) is our expression for the white-noise diffusion while the denominator is the variance in the stochastic force at time t_f . With all quantities now defined, we can begin to discuss the results.

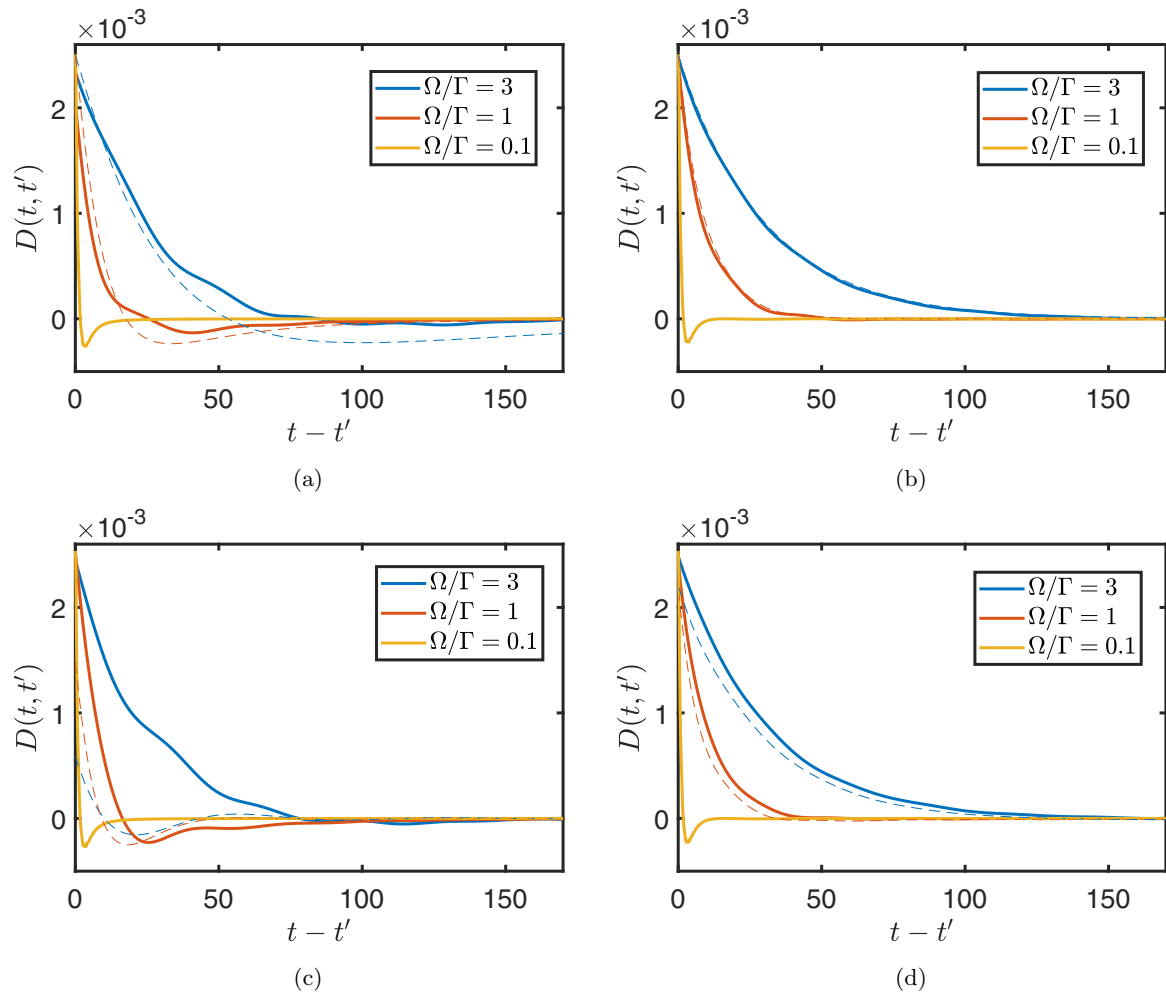


FIG. 9. Exact diffusion coefficient as a function of τ for where time t occurs at: (a) and (b) $x = 0$, (c) and (d) a turning point. Left: $V = 0$, Right: $V = 0.2$. Dashed line is the corresponding $D_{(0)}(t, t')$ for the same parameters.

We once again apply the time-stepping algorithm presented in Sec. II E to find classical Ehrenfest trajectories in time for our classical coordinate. In doing so, we store $A(\omega, t)$ (41) at each time step. The two-time lesser and greater Green's functions can then be computed according to (35) and (36) by inputting $A(\omega, t)$ at different points in the stored trajectory and numerically integrating over ω for each possible value of τ . We then calculate the exact diffusion coefficient as a function of τ according to (60), where $D(\tau = 0)$ corresponds to the variance in the stochastic force at the end point of the trajectory and $D(\tau > 0)$ is the correlation in the stochastic force between the times t and $t - \tau$. To clarify the method, the stochastic force is not included in the simulation. We instead calculate the trajectory using Ehrenfest dynamics as a means to assess the behavior of the exact diffusion coefficient. The common parameters in this section are $\lambda = 0.1$, $k = 1$, and $x_0 = 0$.

In Figs. 9(a)–9(d) we observe the exact diffusion as in (60) for different values of our small parameter (solid line) plotted against the corresponding adiabatic diffusion as per (63) (dashed line). Here time t corresponds to the end point of the trajectory where in Figs. 9(a) and 9(b) the trajectory is ended at a point when $x = 0$, while in Figs. 9(c) and 9(d) the trajectory is ended at a turning point. The left plots are

calculated in equilibrium while the right plots are calculated at a nonzero voltage. The differences between the solid and dashed lines give an indication of the effects of the feedback on the electronic environment due to the motion of the classical coordinate. To our knowledge, the effects of nonadiabatic motion on the diffusion coefficient have not been directly observed previously. As expected, this feedback becomes especially important when the small parameter Ω/Γ becomes larger, such that the perturbative truncation of (60) is no longer satisfied. However, we observe that an increase to the voltage nullifies the effects of the feedback. This is justified by the knowledge that the electronic tunneling timescale is faster at higher voltages [1], meaning that the electronic environment can more readily equilibrate to any changes in the classical geometry. Thus, the timescale separation becomes increasingly justifiable further from equilibrium, even despite Ω/Γ being large. We also find that the correlations in the stochastic force are dissipated over shorter timescales when Ω/Γ is smaller such that $D(\tau)$ approaches a shape more reminiscent of a delta function. Finally, we note that the timescale separation appears less satisfactory at the turning points of the trajectory. The acceleration of the classical coordinate is largest around the turning points and we posit that acceleration dependent terms become important here,

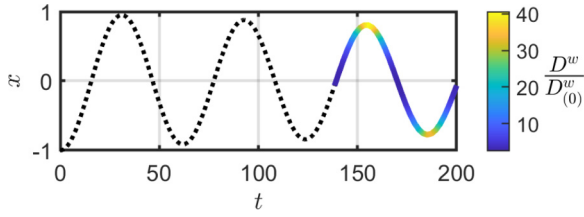


FIG. 10. An example trajectory of the classical coordinate. Color scale shows the calculated $D^w/D_{(0)}^w$ at that point in the trajectory. Parameters: $\Omega/\Gamma = 1$, $V = 0$.

which are otherwise unaccounted for under the assumption of adiabatic motion.

The effectiveness of the timescale separation for different ending positions along the trajectory is quantified in Fig. 10, in which we have calculated $D^w/D_{(0)}^w$ for different end positions along a period of the trajectory when $\Omega/\Gamma = 1$. For these parameters, the timescale separation is ineffective as D^w is over twice as large as $D_{(0)}^w$ at a minimum. We observe the adiabatic assumption to be at its weakest in the vicinity of the turning points.

In Fig. 11 we use t_{corr}/T_p as a measure of the suitability of the white-noise approximation, where T_p is the period of oscillations in the classical coordinate. Here t_{corr} contains any information about the electronic forces acting on the coordinate, while T_p contains information on the classical force. We observe that an increase to Ω/Γ results in a corresponding increase to t_{corr}/T_p , implying that the white-noise approximation is more valid at smaller Ω/Γ where the timescale separation is more well defined. However, we note that the validity decreases upon increasing the voltage which would ordinarily serve to further increase the timescale separation. For this system, a larger voltage results in more persistent correlations in the stochastic force which emerges in the numerator of (67), while the change in the denominator is comparatively irrelevant.

This counterintuitive result also indirectly emerges in Fig. 12 where we observe the white-noise approximation to become more applicable outside of the voltage window and away from the chemical potentials of the leads. In this region,

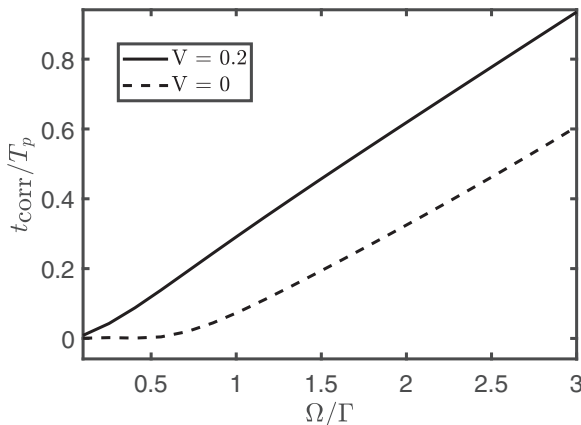


FIG. 11. The ratio of the correlation time to the period of classical oscillation, as a function of Ω/Γ for equilibrium and nonequilibrium cases. Trajectory length = 300.

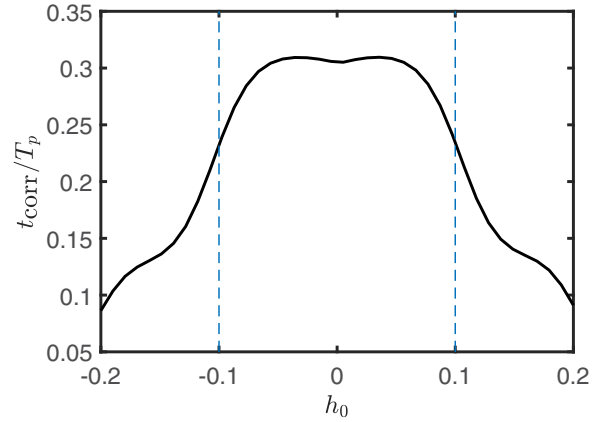


FIG. 12. The ratio of correlation time to the period of classical oscillation for shifted values of h_0 . The dashed blue lines show the edges of the voltage window. Parameters: $\Omega/\Gamma = 1$.

electrons tunnel more slowly through the central region. We do not yet have a convincing explanation for this.

IV. CONCLUSIONS

In this paper we have introduced a time-stepping algorithm for evaluating the exact lesser Green's function at equal times, which allows us to simulate the trajectory of multiple classical coordinates simultaneously via an Ehrenfest approach. We use this to benchmark the commonly used Langevin approach which necessitates the use of a timescale separation between classical and electronic coordinates within the system. We observe that despite our avoidance of a timescale separation within our system, we observe negative dissipations (positive power input to the classical coordinate) as predicted by the Langevin approach. We also note that these negative dissipations can be overwhelmed by positive dissipations due to higher order forces unaccounted for in the Langevin approach. We also apply our method to the calculation of the diffusion coefficient in which we observe the effect of the nonadiabatic feedback of the classical coordinate onto the electronic environment and its behavior under a timescale separation. Additionally, we assess the validity of the white-noise approximation for the diffusion coefficient for a range of parameters and find that it is most applicable under a clear timescale separation within the system and is better applied when the transport channel energy is shifted outside of the voltage window.

APPENDIX A: VISCOSITY COEFFICIENT IN THE SINGLE-LEVEL CASE

For the case of a single electronic level and any number of classical degrees of freedom, the first order force for an arbitrary degree of freedom ν in (19) is given by

$$F_{\nu,(1)} = \int \frac{d\omega}{2\pi} i \partial_\nu h \tilde{G}_{(1)}^<, \quad (\text{A1})$$

where $\tilde{G}_{(1)}^<$ in the single-level case can be simplified to

$$\tilde{G}_{(1)}^< = \frac{i}{2} \partial_T h \tilde{G}_{(0)}^R \tilde{G}_{(0)}^A (\tilde{G}_{(0)}^A - \tilde{G}_{(0)}^R) \partial_\omega \tilde{\Sigma}^<. \quad (\text{A2})$$

Through the use of (23), (28), and the fact that $\partial_\omega f_\alpha = -\frac{1}{T_\alpha} f_\alpha (1 - f_\alpha)$, some simplification yields

$$\tilde{G}_{(1)}^< = \frac{i\partial_T h \Gamma \left[\frac{f_L}{T_L} (1 - f_L) \Gamma_L + \frac{f_R}{T_R} (1 - f_R) \Gamma_R \right]}{2 \left[(\omega - h)^2 + \frac{\Gamma^2}{4} \right]^2}. \quad (\text{A3})$$

We obtain the simplified form of $F_{v,(1)}$ by substituting (A3) into (A1):

$$F_{v,(1)} = -\partial_v h \partial_T h \Gamma \int \frac{d\omega}{4\pi} \frac{\frac{f_L}{T_L} (1 - f_L) \Gamma_L + \frac{f_R}{T_R} (1 - f_R) \Gamma_R}{\left[(\omega - h)^2 + \frac{\Gamma^2}{4} \right]^2}. \quad (\text{A4})$$

We apply the chain rule such that $\partial_T h = \sum_{v'} v_{v'} \partial_{v'} h$ where $v_{v'}$ is the velocity of the v' coordinate and the summation is over all classical degrees of freedom. The diagonal components of the force then correspond to when $v' = v$, for which we will utilize an additional subscript:

$$F_{vv,(1)} = -v_v (\partial_v h)^2 \Gamma \int \frac{d\omega}{4\pi} \frac{\frac{f_L}{T_L} (1 - f_L) \Gamma_L + \frac{f_R}{T_R} (1 - f_R) \Gamma_R}{\left[(\omega - h)^2 + \frac{\Gamma^2}{4} \right]^2}. \quad (\text{A5})$$

Finally, the diagonal components of the viscosity coefficient can then be found according to $\xi_{vv} = -\frac{F_{vv,(1)}}{v_v}$, which yields

$$\xi_{vv} = \frac{\Gamma (\partial_v h)^2}{4\pi} \int d\omega \frac{\frac{f_L}{T_L} (1 - f_L) \Gamma_L + \frac{f_R}{T_R} (1 - f_R) \Gamma_R}{\left[(\omega - h)^2 + \frac{\Gamma^2}{4} \right]^2}. \quad (\text{A6})$$

APPENDIX B: EXACT DIFFUSION COEFFICIENT

Here we derive (60) for the case of a single electronic level and single classical degree of freedom x . We express the quantum force acting on the classical coordinate due to the electronic environment according to a mean component which contains the deterministic forces, and a stochastic component which captures the probabilistic fluctuations about the mean:

$$\hat{f}(t) = f(t) + \delta \hat{f}(t). \quad (\text{B1})$$

By multiplying this equation by itself at a different time t' and utilizing the fact that $\langle \delta \hat{f}(t) \rangle = 0$, we find

$$\langle \delta \hat{f}(t) \delta \hat{f}(t') \rangle = \langle \hat{f}(t) \hat{f}(t') \rangle - f(t) f(t'), \quad (\text{B2})$$

where the quantum force operator according to (7) is given by

$$\hat{f}(t) = -\partial_x U - \partial_x h d^\dagger d. \quad (\text{B3})$$

After inputting this expression into (B2) and applying Wick's theorem to decompose the strings of creation and annihilation operators, we observe that the terms in $f(t) f(t')$ cancel exactly with part of the decomposition of $\langle \hat{f}(t) \hat{f}(t') \rangle$. We are then left with

$$\langle \delta \hat{f}(t) \delta \hat{f}(t') \rangle = (\partial_x h)^2 \langle d^\dagger(t) d(t') \rangle \langle d(t) d^\dagger(t') \rangle \quad (\text{B4})$$

$$= \lambda^2 G^>(t, t') G^<(t', t). \quad (\text{B5})$$

Here we have used the fact that $\partial_x h = \lambda$ for our model and we have utilized the definitions for the lesser and greater Green's functions.

APPENDIX C: WIGNER TRANSFORM OF (60)

Direct application of the Wigner transform to (60) yields

$$\tilde{D}(\omega, T) = \lambda^2 \int d\tau e^{i\omega\tau} G^>(t, t') G^<(t', t). \quad (\text{C1})$$

Now we replace $G^<$ in the time domain by the inverse Wigner transform of $\tilde{G}^<$ and simplify to find

$$\tilde{D}(\omega, T) = \frac{\lambda^2}{2\pi} \int d\tau e^{i\omega\tau} G^>(t, t') \int d\omega' e^{-i\omega'(-\tau)} \tilde{G}^<(\omega', T) \quad (\text{C2})$$

$$= \frac{\lambda^2}{2\pi} \int d\omega' \int d\tau e^{i(\omega+\omega')\tau} G^>(t, t') \tilde{G}^<(\omega', T) \quad (\text{C3})$$

$$= \frac{\lambda^2}{2\pi} \int d\omega' \tilde{G}^>(\omega + \omega', T) \tilde{G}^<(\omega', T), \quad (\text{C4})$$

where we have used the definition of the Wigner transform.

APPENDIX D: EQUATION FOR THE WHITE-NOISE DIFFUSION

In (64) we introduced the white-noise diffusion D^w as a means of representing the colored-noise diffusion in a Markovian manner. We are then tasked with finding an equation for D^w whose application will accurately reproduce the dynamics produced by the exact colored-noise diffusion. To do so, we consider a pedagogical example in which we neglect all forces except the stochastic force. The governing equation of motion is given by

$$m \frac{dv}{dt} = \delta f(t). \quad (\text{D1})$$

This is solved for the velocity at time t according to

$$v(t) = v(0) + \frac{1}{m} \int_0^t dt' \delta f(t'). \quad (\text{D2})$$

The change in kinetic energy of the classical coordinate is then found by squaring the above and taking an average over the fluctuations such that we obtain

$$\Delta KE = \frac{1}{2m} \int_0^t dt' \int_0^t dt'' D(t', t''). \quad (\text{D3})$$

Now we implement the white-noise approximation according to (64) and solve for an equation for D^w which yields the same change in kinetic energy. Making the transformation from (t', t'') to (T, τ) yields

$$\Delta KE = \frac{1}{2m} \int_0^t dT \int_{-T}^T d\tau D^w(T) \delta(\tau) \quad (\text{D4})$$

$$= \frac{1}{2m} \int_0^t dT D^w(T). \quad (\text{D5})$$

By enforcing that (D5) and (D3) are equal, we find

$$\int_0^t dT D^w(T) = \int_0^t dT \int_{-T}^T d\tau D(T, \tau). \quad (\text{D6})$$

Application of $\frac{d}{dt}$ to both sides and using the symmetry property, $D(T, \tau) = D(T, -\tau)$, then yields

$$D^w(t) = \int_{-t}^t d\tau D(t, \tau) + 2 \int_0^t dT D(T, t). \quad (\text{D7})$$

Finally, we assume that time t is sufficiently large such that $D(T, t)$ is approximately zero. This amounts to assuming that the correlations in the stochastic force decay to zero over time intervals of t or longer. The second term disappears and we are left with our final expression for the white-noise diffusion coefficient:

$$D^w(t) = \int_{-t}^t d\tau D(t, \tau). \quad (\text{D8})$$

Clearly the white-noise approximation in this case will produce the same observable change in kinetic energy over any timescale. However, the inclusion of a frictional force and an external potential will limit the validity of the approximation to finite timescales dependent on their respective strengths. This is because these forces may produce an appreciable effect on the dynamics over the timescales for which the stochastic force is correlated.

- [1] J. C. Cuevas and E. Scheer, *Molecular Electronics*, World Scientific Series in Nanoscience and Nanotechnology Vol. 15 (World Scientific, Singapore, 2017).
- [2] D. R. Ward, D. A. Corley, J. M. Tour, and D. Natelson, Vibrational and electronic heating in nanoscale junctions, *Nat. Nanotechnol.* **6**, 33 (2011).
- [3] C. Sabater, C. Untiedt, and J. M. van Ruitenbeek, Evidence for non-conservative current-induced forces in the breaking of Au and Pt atomic chains, *Beilst. J. Nanotechnol.* **6**, 2338 (2015).
- [4] M. Tsutsui, M. Taniguchi, and T. Kawai, Local heating in metal-molecule-metal junctions, *Nano Lett.* **8**, 3293 (2008).
- [5] G. Schulze, K. J. Franke, A. Gagliardi, G. Romano, C. S. Lin, A. L. Rosa, T. A. Niehaus, T. Frauenheim, A. Di Carlo, A. Pecchia, and J. I. Pascual, Resonant Electron Heating and Molecular Phonon Cooling in Single C₆₀ Junctions, *Phys. Rev. Lett.* **100**, 136801 (2008).
- [6] Z. Ioffe, T. Shamai, A. Ophir, G. Noy, I. Yutsis, K. Kfir, O. Cheshnovsky, and Y. Selzer, Detection of heating in current-carrying molecular junctions by Raman scattering, *Nat Nanotechnol.* **3**, 727 (2008).
- [7] K. J. Franke and J. I. Pascual, Effects of electron-vibration coupling in transport through single molecules, *J. Phys.: Condens. Matter* **24**, 394002 (2012).
- [8] S. Mukherjee, F. Libisch, N. Large, O. Neumann, L. V. Brown, J. Cheng, J. B. Lassiter, E. A. Carter, P. Nordlander, and N. J. Halas, Hot electrons do the impossible: Plasmon-induced dissociation of H₂ on Au, *Nano Lett.* **13**, 240 (2013).
- [9] Z. Huang, B. Xu, Y. Chen, M. D. Ventra, and N. J. Tao, Measurement of current-induced local heating in a single molecule junction, *Nano Lett.* **6**, 1240 (2006).
- [10] N. P. de Leon, W. Liang, Q. Gu, and H. Park, Vibrational excitation in single-molecule transistors: Deviation from the simple Franck-Condon prediction, *Nano Lett.* **8**, 2963 (2008).
- [11] A. K. Hüttel, B. Witkamp, M. Leijnse, M. R. Wegewijs, and H. S. J. van der Zant, Pumping of Vibrational Excitations in the Coulomb-Blockade Regime in a Suspended Carbon Nanotube, *Phys. Rev. Lett.* **102**, 225501 (2009).
- [12] J. Stettenheim, M. Thalakulam, F. Pan, and Others, A macroscopic mechanical resonator driven by mesoscopic electrical back-action., *Nature (London)* **466**, 86 (2010).
- [13] G. Schulze, K. J. Franke, and J. I. Pascual, Resonant heating and substrate-mediated cooling of a single C₆₀ molecule in a tunnel junction, *New J. Phys.* **10**, 065005 (2008).
- [14] J. R. Hahn and W. Ho, Chemisorption and dissociation of single oxygen molecules on Ag(110), *J. Chem. Phys.* **123**, 214702 (2005).
- [15] S. Roy, V. Mujica, and M. A. Ratner, Chemistry at molecular junctions: Rotation and dissociation of O₂ on the Ag(110) surface induced by a scanning tunneling microscope, *J. Chem. Phys.* **139**, 074702 (2013).
- [16] S.-W. Hla, L. Bartels, G. Meyer, and K.-H. Rieder, Inducing All Steps of a Chemical Reaction with the Scanning Tunneling Microscope Tip: Towards Single Molecule Engineering, *Phys. Rev. Lett.* **85**, 2777 (2000).
- [17] L. J. Lauhon and W. Ho, Control and Characterization of a Multistep Unimolecular Reaction, *Phys. Rev. Lett.* **84**, 1527 (2000).
- [18] B. C. Stipe, M. A. Rezaei, W. Ho, S. Gao, M. Persson, and B. I. Lundqvist, Single-Molecule Dissociation by Tunneling Electrons, *Phys. Rev. Lett.* **78**, 4410 (1997).
- [19] H. Li, T. A. Su, V. Zhang, M. L. Steigerwald, C. Nuckolls, and L. Venkataraman, Electric field breakdown in single molecule junctions, *J. Am. Chem. Soc.* **137**, 5028 (2015).
- [20] H. Li, N. T. Kim, T. A. Su, M. L. Steigerwald, C. Nuckolls, P. Darancet, J. L. Leighton, and L. Venkataraman, Mechanism for Si-Si bond rupture in single molecule junctions, *J. Am. Chem. Soc.* **138**, 16159 (2016).
- [21] I. V. Pobelov, K. P. Lauritzen, K. Yoshida, A. Jensen, G. Mészáros, K. W. Jacobsen, M. Strange, T. Wandlowski, and G. C. Solomon, Dynamic breaking of a single gold bond, *Nat. Commun.* **8**, 15931 (2017).
- [22] G.-H. Ding, B. Xiong, and B. Dong, Transient currents of a single molecular junction with a vibrational mode, *J. Phys.: Condens. Matter* **28**, 065301 (2016).
- [23] A. Erpenbeck, R. Härtle, M. Bockstedte, and M. Thoss, Vibrationally dependent electron-electron interactions in resonant electron transport through single-molecule junctions, *Phys. Rev. B* **93**, 115421 (2016).
- [24] C. Schinabeck, R. Härtle, H. B. Weber, and M. Thoss, Current noise in single-molecule junctions induced by electronic-vibrational coupling, *Phys. Rev. B* **90**, 075409 (2014).
- [25] F. Haupt, T. Novotný, and W. Belzig, Current noise in molecular junctions: Effects of the electron-phonon interaction, *Phys. Rev. B* **82**, 165441 (2010).
- [26] M. Galperin, K. Saito, A. V. Balatsky, and A. Nitzan, Cooling mechanisms in molecular conduction junctions, *Phys. Rev. B* **80**, 115427 (2009).
- [27] A. Erpenbeck and M. Thoss, Hierarchical quantum master equation approach to vibronic reaction dynamics at metal surfaces, *J. Chem. Phys.* **151**, 191101 (2019).
- [28] J. Koch, M. Semmelhack, F. von Oppen, and A. Nitzan, Current-induced nonequilibrium vibrations in single-molecule devices, *Phys. Rev. B* **73**, 155306 (2006).
- [29] E. Y. Wilner, H. Wang, M. Thoss, and E. Rabani, Nonequilibrium quantum systems with electron-phonon interactions: Transient dynamics and approach to steady state, *Phys. Rev. B* **89**, 205129 (2014).

- [30] H. Wang, I. Pshenichnyuk, R. Härtle, and M. Thoss, Numerically exact, time-dependent treatment of vibrationally coupled electron transport in single-molecule junctions, *J. Chem. Phys.* **135**, 244506 (2011).
- [31] C. Schinabeck, A. Erpenbeck, R. Härtle, and M. Thoss, Hierarchical quantum master equation approach to electronic-vibrational coupling in nonequilibrium transport through nanosystems, *Phys. Rev. B* **94**, 201407(R) (2016).
- [32] R. J. Preston, V. F. Kershaw, and D. S. Kosov, Current-induced atomic motion, structural instabilities, and negative temperatures on molecule-electrode interfaces in electronic junctions, *Phys. Rev. B* **101**, 155415 (2020).
- [33] R. J. Preston, T. D. Honeychurch, and D. S. Kosov, Cooling molecular electronic junctions by AC current, *J. Chem. Phys.* **153**, 121102 (2020).
- [34] V. F. Kershaw and D. S. Kosov, Non-adiabatic effects of nuclear motion in quantum transport of electrons: A self-consistent Keldysh-Langevin study, *J. Chem. Phys.* **153**, 154101 (2020).
- [35] G. Micchi, R. Avriller, and F. Pistolesi, Electromechanical transition in quantum dots, *Phys. Rev. B* **94**, 125417 (2016).
- [36] J.-T. Lu, M. Brandbyge, and P. Hedegård, Blowing the fuse: Berry's phase and runaway vibrations in molecular conductors, *Nano Lett.* **10**, 1657 (2010).
- [37] J.-T. Lü, R. B. Christensen, J.-S. Wang, P. Hedegård, and M. Brandbyge, Current-Induced Forces and Hot Spots in Biased Nanojunctions, *Phys. Rev. Lett.* **114**, 096801 (2015).
- [38] A. Erpenbeck, C. Schinabeck, U. Peskin, and M. Thoss, Current-induced bond rupture in single-molecule junctions, *Phys. Rev. B* **97**, 235452 (2018).
- [39] A. A. Dzhioev, D. S. Kosov, and F. von Oppen, Out-of-equilibrium catalysis of chemical reactions by electronic tunnel currents, *J. Chem. Phys.* **138**, 134103 (2013).
- [40] A. A. Dzhioev and D. S. Kosov, Kramers problem for nonequilibrium current-induced chemical reactions, *J. Chem. Phys.* **135**, 074701 (2011).
- [41] R. J. Preston, M. F. Gelin, and D. S. Kosov, First-passage time theory of activated rate chemical processes in electronic molecular junctions, *J. Chem. Phys.* **154**, 114108 (2021).
- [42] W. Dou, G. Miao, and J. E. Subotnik, Born-Oppenheimer Dynamics, Electronic Friction, and the Inclusion of Electron-Electron Interactions, *Phys. Rev. Lett.* **119**, 046001 (2017).
- [43] W. Dou and J. E. Subotnik, Universality of electronic friction. II. Equivalence of the quantum-classical Liouville equation approach with von Oppen's nonequilibrium Green's function methods out of equilibrium, *Phys. Rev. B* **97**, 064303 (2018).
- [44] N. Bode, S. V. Kusminskiy, R. Egger, and F. von Oppen, Current-induced forces in mesoscopic systems: A scattering-matrix approach, *Beilst. J. Nanotechnol.* **3**, 144 (2012).
- [45] F. Chen, K. Miwa, and M. Galperin, Current-induced forces for nonadiabatic molecular dynamics, *J. Phys. Chem. A* **123**, 693 (2019).
- [46] F. Chen, K. Miwa, and M. Galperin, Electronic friction in interacting systems, *J. Chem. Phys.* **150**, 174101 (2019).
- [47] J.-T. Lü, M. Brandbyge, P. Hedegård, T. N. Todorov, and D. Dundas, Current-induced atomic dynamics, instabilities, and Raman signals: Quasiclassical Langevin equation approach, *Phys. Rev. B* **85**, 245444 (2012).
- [48] A. Nocera, C. A. Perroni, V. Marigliano Ramaglia, and V. Cataudella, Stochastic dynamics for a single vibrational mode in molecular junctions, *Phys. Rev. B* **83**, 115420 (2011).
- [49] D. Dundas, E. J. McEniry, and T. N. Todorov, Current-driven atomic waterwheels, *Nat. Nanotechnol.* **4**, 99 (2009).
- [50] D. Dundas, B. Cunningham, C. Buchanan, A. Terasawa, A. T. Paxton, and T. N. Todorov, An ignition key for atomic-scale engines, *J. Phys.: Condens. Matter* **24**, 402203 (2012).
- [51] B. Cunningham, T. N. Todorov, and D. Dundas, Nonconservative dynamics in long atomic wires, *Phys. Rev. B* **90**, 115430 (2014).
- [52] J.-T. Lü, T. Gunst, P. Hedegård, and M. Brandbyge, Current-induced dynamics in carbon atomic contacts, *Beilst. J. Nanotechnol.* **2**, 814 (2011).
- [53] R. B. Christensen, J.-T. Lü, P. Hedegård, and M. Brandbyge, Current-induced runaway vibrations in dehydrogenated graphene nanoribbons, *Beilst. J. Nanotechnol.* **7**, 68 (2016).
- [54] R. Hussein, A. Metelmann, P. Zedler, and T. Brandes, Semiclassical dynamics of nanoelectromechanical systems, *Phys. Rev. B* **82**, 165406 (2010).
- [55] M. Hopjan, G. Stefanucci, E. Perfetto, and C. Verdozzi, Molecular junctions and molecular motors: Including Coulomb repulsion in electronic friction using nonequilibrium Green's functions, *Phys. Rev. B* **98**, 041405(R) (2018).
- [56] A. Kartsev, C. Verdozzi, and G. Stefanucci, Nonadiabatic Van der Pol oscillations in molecular transport, *Eur. Phys. J. B* **87**, 14 (2014).
- [57] G. Foti and H. Vázquez, Origin of vibrational instabilities in molecular wires with separated electronic states, *J. Phys. Chem. Lett.* **9**, 2791 (2018).
- [58] T. Gunst, J.-T. Lü, P. Hedegård, and M. Brandbyge, Phonon excitation and instabilities in biased graphene nanoconstrictions, *Phys. Rev. B* **88**, 161401 (2013).
- [59] L. Simine and D. Segal, Vibrational cooling, heating, and instability in molecular conducting junctions: Full counting statistics analysis, *Phys. Chem. Chem. Phys.* **14**, 13820 (2012).
- [60] R. Härtle and M. Thoss, Vibrational instabilities in resonant electron transport through single-molecule junctions, *Phys. Rev. B* **83**, 125419 (2011).
- [61] J.-T. Lü, P. Hedegård, and M. Brandbyge, Laserlike Vibrational Instability in Rectifying Molecular Conductors, *Phys. Rev. Lett.* **107**, 046801 (2011).
- [62] V. Rizzi, T. N. Todorov, J. J. Kohanoff, and A. A. Correa, Electron-phonon thermalization in a scalable method for real-time quantum dynamics, *Phys. Rev. B* **93**, 024306 (2016).
- [63] A. Nitzan and M. Galperin, Kinetic schemes in open interacting systems, *J. Phys. Chem. Lett.* **9**, 4886 (2018).
- [64] P. Hyldgaard, Nonequilibrium thermodynamics of interacting tunneling transport: Variational grand potential, density functional formulation and nature of steady-state forces, *J. Phys.: Condens. Matter* **24**, 424219 (2012).
- [65] T. N. Todorov, D. Dundas, and E. J. McEniry, Nonconservative generalized current-induced forces, *Phys. Rev. B* **81**, 075416 (2010).
- [66] C. Verdozzi, G. Stefanucci, and C.-O. Almbladh, Classical Nuclear Motion in Quantum Transport, *Phys. Rev. Lett.* **97**, 046603 (2006).
- [67] M. Brandbyge, K. Stokbro, J. Taylor, J. L. Mozos, and P. Ordejón, Origin of current-induced forces in an atomic gold wire: A first-principles study, *Phys. Rev. B* **67**, 193104 (2003).

- [68] A. Metelmann and T. Brandes, Adiabaticity in semiclassical nanoelectromechanical systems, *Phys. Rev. B* **84**, 155455 (2011).
- [69] A. P. Horsfield, D. R. Bowler, A. J. Fisher, T. N. Todorov, and M. J. Montgomery, Power dissipation in nanoscale conductors: Classical, semi-classical and quantum dynamics, *J. Phys.: Condens. Matter* **16**, 3609 (2004).
- [70] E. J. McEniry, D. R. Bowler, D. Dundas, A. P. Horsfield, C. G. Sánchez, and T. N. Todorov, Dynamical simulation of inelastic quantum transport, *J. Phys.: Condens. Matter* **19**, 196201 (2007).
- [71] A. P. Horsfield, D. R. Bowler, A. J. Fisher, T. N. Todorov, and C. G. Sánchez, Beyond Ehrenfest: Correlated non-adiabatic molecular dynamics, *J. Phys.: Condens. Matter* **16**, 8251 (2004).
- [72] A. Nitzan, *Chemical Dynamics in Condensed Phases* (Oxford University Press, Oxford, 2006).
- [73] T. N. Todorov, D. Dundas, J.-T. Lü, M. Brandbyge, and P. Hedegård, Current-induced forces: A simple derivation, *Eur. J. Phys.* **35**, 065004 (2014).
- [74] J.-T. Lü, B.-Z. Hu, P. Hedegård, and M. Brandbyge, Semi-classical generalized Langevin equation for equilibrium and nonequilibrium molecular dynamics simulation, *Prog. Surf. Sci.* **94**, 21 (2019).
- [75] A. P. Jauho, N. S. Wingreen, and Y. Meir, Time-dependent transport in interacting and noninteracting resonant-tunneling systems, *Phys. Rev. B* **50**, 5528 (1994).
- [76] D. A. McQuarrie, *Quantum Chemistry*, 2nd ed. (University Science Books, Melville, NY, 2008).